Mode Locking in Reversed-Field Pinch Experiments

H. K. Ebraheem and J. L. Shohet
University of Wisconsin–Madison, Madison, Wisconsin 53706

A. C. Scott
University of Arizona, Tucson, Arizona 85721

(Received 16 November 2001; revised manuscript received 3 May 2002; published 24 May 2002)

The MHD mode trajectory in the Madison Symmetric Torus reversed-field pinch has been found to obey the sine-Gordon equation. Corresponding to experiment, a perturbation analysis predicts the locations of mode locking to be at the vacuum chamber poloidal and/or toroidal gaps. The mode's energy dissipates when it locks, as shown by a decaying spiral phase-plane trajectory. Unlocked modes travel around the torus without an abrupt energy loss. By varying key machine parameters obtained by statistical analysis, the probability of locking in accordance with the experimental results can be predicted.

DOI: 10.1103/PhysRevLett.88.235003 PACS numbers: 52.55.Lf

The purpose of this Letter is to introduce a model that describes the motion of the localized MHD mode that has been observed to travel between the magnetic surfaces just inside the reversal layer in the reversed-field pinch experiment at the University of Wisconsin–Madison, the Madison Symmetric Torus (MST). The model is used to predict: (i) the conditions for locking of the MHD mode based on experimental results and (ii) the probability of a discharge locking as a function of key variables.

The MST experiment is a large reversed-field pinch with a minor radius of 0.52 m and a major radius of 1.5 m [1]. The aluminum toroidal vacuum chamber wall is 0.05 m thick except for two insulating gaps: one that cuts the vacuum chamber toroidally and one that cuts the chamber poloidally. Voltages can be set and/or measured across these gaps. The equation of motion for the MHD mode can be obtained by summing torques [2–5] acting on the mode around the magnetic axis. In particular, those torques that are proportional to the confining magnetic fields vary sinusoidally [4] around the mode trajectory due to the toroidal effect. Depending upon the values of various parameters, the probability of locking (the mode becomes stationary and causes the discharge to expel its energy) increases.

Because identical operating conditions did not always show locking from shot to shot, and in order to determine the significance of the discharge variables, a binary logistical regression analysis [6] of 4492 MST discharges was performed. The analysis indicated which of seven variables had the strongest effect on the probability of locking. The four statistically most significant variables were found to be I_P, the induced plasma current; V_{TG}, the voltage across the toroidal gap; V_{PG}, the voltage across the poloidal gap; and V_{loop}, the loop voltage around the torus. Table I shows the coefficients obtained from the logistical regression analysis [6].

In Table I, the sign of the coefficients determines whether the probability of locking increases or decreases as the predictor variable increases. The p value determines whether these variables are statistically significant. In this analysis, any p value of magnitude less than 0.05 is statistically significant. Thus, increasing I_P, V_{PG}, and V_{TG} increases the probability of locking while increasing V_{loop} decreases the probability of locking.

Experimentally, it was found that the mode locked at or near the intersection of the poloidal and toroidal gaps. The trajectory of the mode may not always pass over this intersection during its motion around the torus, depending on the mode's rotational transform at the minor radius where the mode is located. Eventually, it does pass close enough to the intersection of the gaps so that locking occurs, provided that the mode-driving torque and the mode dissipation are of the proper levels to permit locking.

Based on the observed properties of the MHD mode along with an analysis of the torques around the magnetic axis acting on the mode, we propose that it behaves as a kink soliton, which is a solution of the sine-Gordon equation. Such kink solitons have been studied in the case of the propagation of a fluxon along a Josephson-junction transmission line (JTL) [7–10], and we shall follow a similar analysis here.

In order to develop the sine-Gordon equation model, we make the following assumptions about the nature of the MHD mode. First, we assume that the mode is generated by magnetic reconnection and is an isolated magnetic island of finite length that wraps around the magnetic axis of the torus as shown in Fig. 1. Just as is the case in the main magnetic confinement surfaces, we assume that there is a component of the current in the island that flows poloidally around its magnetic surfaces producing magnetic moments

TABLE I. Statistical coefficients obtained by logistical regression analysis.

Predictor	Coefficient	p Value
I_P	0.058245	<0.001
V_{loop}	-0.05649	<0.001
V_{PG}	0.03482	<0.001
V_{TG}	0.08045	<0.001

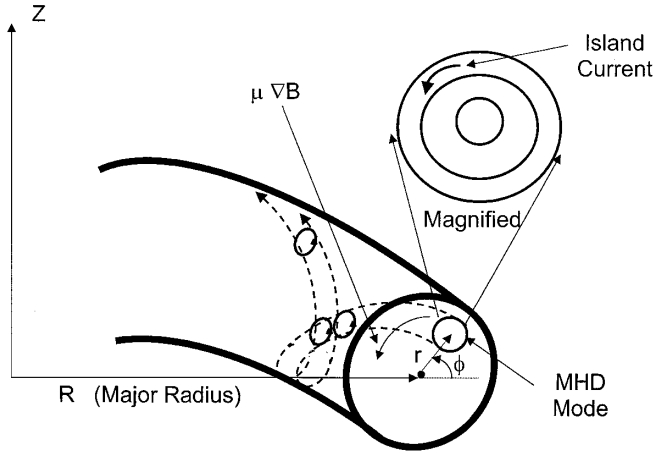

FIG. 1. A conceptual drawing of the MHD kink mode in the MST torus. The mode threads its way along the torus passing both the poloidal and toroidal vacuum chamber gaps.

along the length of the island. We further assume that the dominant magnetic fields at the location of the island vary toroidally as shown in Eq. (1):

$$B = \frac{B_0}{1 - \frac{r}{R}\cos\phi} \cong B_0\left[1 + \frac{r}{R}\cos\phi\right], \qquad (1)$$

where r is the minor radius to the island, R is the major radius of the torus, and ϕ is the poloidal angle that can be used to locate the island at each position along its length. A force in the ϕ direction results from the $\mu\Delta B$ force acting on the magnetic moments of the island with a resulting torque around the magnetic axis of

$$\text{torque} = -\mu B_0 (r/R)\sin\phi\,. \qquad (2)$$

Since the island is long enough so that the circulating current around the island magnetic surfaces may be considered to be a solenoid, then each incremental section of the island can be considered as a circular loop around which the current flows. The magnetic forces on each loop act so as to align the loops. Thus, any twisting of the loops will result in a springlike restoring torque to realign them.

Accordingly, we sum torques around the magnetic axis to produce the sine-Gordon equation

$$M\frac{\partial^2\phi}{\partial t^2} = K\frac{\partial^2\phi}{\partial x^2} - T\sin\phi\,, \qquad (3)$$

where M is the mass per unit length of the MHD mode, K is the spring restoring torque constant for the individual loops, T is the torque constant due to the external magnetic field from Eq. (2), and x is the helical distance along the MHD mode trajectory. We now must include the effects of viscous damping and the drive term that make the MHD mode move around the torus as well as the presence of the vacuum chamber gaps. We include these effects after normalizing Eq. (3) by adding a perturbation term as follows:

$$\frac{\partial^2\psi}{\partial t^2} = \frac{\partial^2\psi}{\partial x^2} - \sin\psi + \varepsilon f\,, \qquad (4)$$

where ψ is the normalized angle that describes the position and velocity of the MHD mode, and the perturbation term is

$$\varepsilon f = -\alpha\frac{\partial\psi}{\partial t} - \gamma - \mu\sum_i \delta(x\cos\theta - 2\pi iR)\sin\psi - k\sum_j \delta(x\sin\theta - 2\pi jr_0)\sin\psi\,. \qquad (5)$$

In Eq. (5), the first term on the right, with coefficient α, is due to viscous damping which is produced by resistive MHD effects. The second term, γ, is the driving term which we assume is proportional to V_{loop}. Recall that the logistical regression analysis of the experimental data shows that V_{loop} is inversely correlated with locking, which is exactly what the calculations will show. The delta function terms on the right-hand side of Eq. (5) are potential hills or potential wells which are used to represent the toroidal and poloidal gaps which produce field errors along the trajectory of the mode. If all of these effects balance on the average, the mode travels at a constant average velocity. The summations are required to account for multiple encounters of the poloidal and toroidal gaps as the mode travels along its helical path. The magnitudes of the coefficients μ and k are proportional to the magnitudes of the field errors across the respective gaps which are determined by I_{P}, V_{TG}, and V_{PG}. i and j are integers. The signs of μ and k determine whether the gap acts as a potential well or a potential hill. We have chosen the rotation number and starting point of the mode so that it does not initially pass the point where both gaps intersect. A negative sign indicates a potential well. Θ is the angle the mode trajectory makes with the midplane of the torus and r_0 is the minor radius of the vacuum chamber.

As the MHD mode moves toward a hill, it slows down and can be reflected. As it passes toward a well, it speeds up but can be trapped (locked) close to the bottom

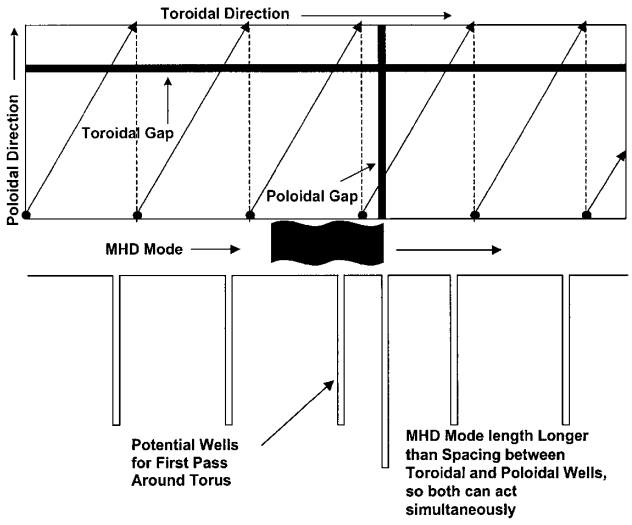

FIG. 2. MHD mode trajectory showing locations of gaps and potential wells.

of the well, provided the dissipation term is sufficiently large or the driving term is sufficiently small so that the mode does not gain enough energy from the driver to leave the well.

Figure 2 shows the "unwrapped" MST torus showing a mode trajectory and the locations of the poloidal and toroidal gaps. Whenever the mode trajectory passes a gap, it encounters a potential well as shown below the mode trajectory. Since the MHD mode is a soliton, it has both temporal and spatial extent and thus can overlap more than one well at a given instant and is more likely to be trapped at such locations. This is particularly important when the mode passes close to the intersection of the poloidal and toroidal gaps since the well separation may be less than between other potential wells.

Following Ref. [11], we obtain the following equations of motion for the perturbed sine-Gordon equation:

$$\frac{dv}{dt} = \frac{\pi\gamma}{4}(1 - v^2)^{3/2} - \alpha v(1 - v^2) + \frac{1}{2}\mu(1 - v^2)\sum_i \operatorname{sech}^2\left(\frac{x - ia}{\sqrt{1 - v^2}}\right)\tanh\left(\frac{x - ia}{\sqrt{1 - v^2}}\right) + \frac{1}{2}k(1 - v^2)\sum_j \operatorname{sech}^2\left(\frac{x - jb}{\sqrt{1 - v^2}}\right)\tanh\left(\frac{x - jb}{\sqrt{1 - v^2}}\right) \tag{6}$$

$$\frac{dx}{dt} = v - \frac{1}{2}\mu v\sum_i (x - ja)\operatorname{sech}^2\left(\frac{x - ia}{\sqrt{1 - v^2}}\right)\tanh\left(\frac{x - ia}{\sqrt{1 - v^2}}\right) + \frac{1}{2}kv\sum_j (x - jb)\operatorname{sech}^2\left(\frac{x - jb}{\sqrt{1 - v^2}}\right)\tanh\left(\frac{x - jb}{\sqrt{1 - v^2}}\right). \tag{7}$$

v is the velocity of the centroid of the mode, and x is the position of the centroid of the mode. a and b are the poloidal and toroidal distances around the torus at the location of the MHD mode.

Figure 3 shows the solution of Eqs. (6) and (7) for both a potential hill and a potential well either of which are always located at the point $x = 0$. The mode travels upward in this representation. The dashed lines represent the hill case and the solid lines represent the well case. For the hill condition, the velocity of the mode decreases as it approaches the hill and then increases, if it has enough energy to overcome the hill. If not, it is reflected. In the latter case, in the presence of sufficient dissipation α, the mode can be "pinned" [11] to a position below the hill where the external driving force γ balances the reflective force from the hill. In the trajectories for a well, it can be seen that the velocity increases as the mode approaches the well. If the initial velocity is small enough and/or the dissipative term large enough, the dissipative term lowers the stored energy sufficiently so that the mode cannot escape the well. The mode traps itself close to the point $x = 0$ corresponding to the degradation of the mode observed experimentally [12]. The actual trapping point is slightly greater than $x = 0$ since the reflection force from the wall of the potential well must be large enough to balance the driver term. To eliminate either pinning or trapping, Fig. 3 shows that it is sufficient to increase the initial velocity of the mode. It then exhibits only a decrease (increase) followed by an increase (decrease) in velocity as it passes the hill (well).

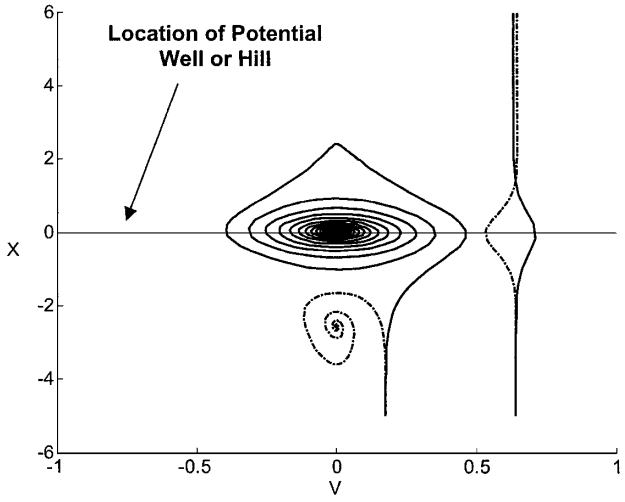

FIG. 3. Phase-plane plots of the MHD mode trajectories for a single potential hill (dashed lines) and for a single potential well (solid lines) at $x = 0$. α was 0.033 for all trajectories; γ was 0.0075 for the locking trajectories and 0.035 for the nonlocking trajectories. μ was +0.5 for the hill case and −0.5 for the well case.

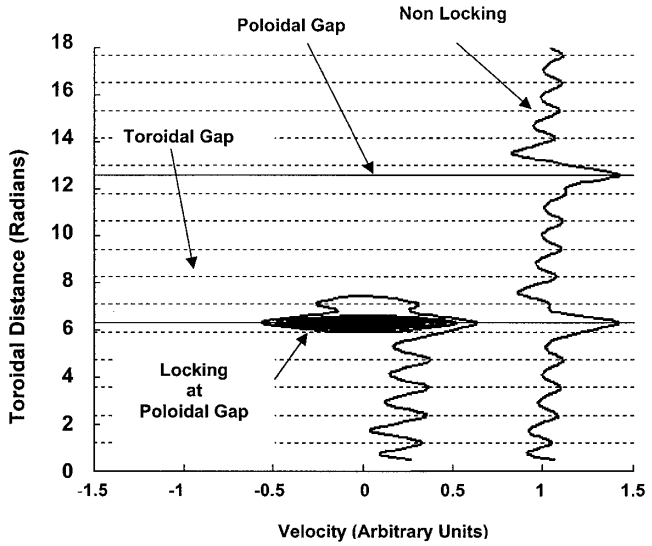

FIG. 4. Phase-plane plots of the MHD mode trajectories along the torus showing both locking and nonlocking trajectories. The horizontal lines show the locations of the poloidal and toroidal gaps.

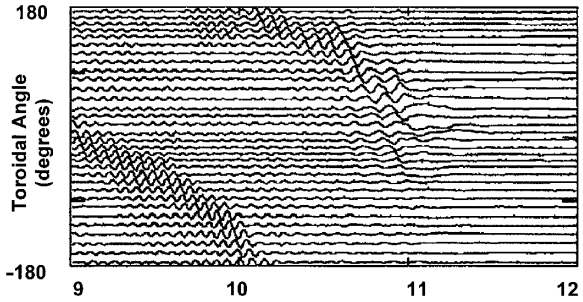

FIG. 5. Experimental detection of MHD mode locking in the MST device. The mode disappears just slightly past the poloidal gap located at a toroidal angle of zero degrees (halfway between the top and bottom of the figure). The horizontal axis is in msec.

We thus conclude that the gaps act as potential wells whose depths are proportional to the field errors at the gaps. The field errors are strongly influenced by the plasma current, I_P, which in turn is also influenced by the gap voltages V_{TG} and V_{PG}.

Figure 4 shows two computed trajectories of the MHD mode for both locking and nonlocking conditions. The values of μ, k, α, and γ were adjusted to produce locking. By slightly increasing the value of γ, decreasing the value of α, and/or decreasing the values of μ and k, the trajectory around the torus can be made nonlocking, as shown in Fig. 4. Conversely, increasing μ and k produce locking. This is what is observed experimentally since lower gap voltages (field errors) decrease the probability of locking. The nonlocking trajectory has been shifted to the right for clarity. The horizontal lines show the locations of the toroidal (dotted lines) and poloidal (solid lines) gaps that the mode encounters during its trajectory. There is a much larger change in velocity when the MHD mode passes near the intersection of both the toroidal and poloidal gaps since, because of the finite extent of the mode, both gaps can operate simultaneously on the mode.

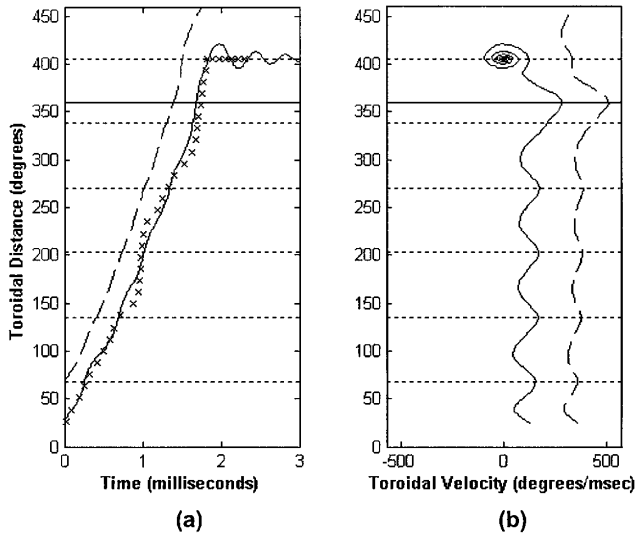

FIG. 6. (a) A summary of locking and nonlocking conditions compared with experimental data. The experimental points are x's. (b) A distance versus velocity phase-plane plot for the same conditions as in (a). For clarity, the nonlocking trajectories are shifted upwards in (a) and to the right in (b).

Figure 5 shows the experimental results in MST [12] when the mode locks. The signals were detected with 32 pickup coils arranged uniformly toroidally around the experiment at a fixed poloidal angle. To compare this with the theory, the average time for the MHD mode to pass each of the pickup coils was obtained and plotted as toroidal angle versus time in Fig. 6a with the solid curves being the theory. It can be straightforwardly fit to the data because, in the experiment, locking occurs at the first toroidal gap just past the poloidal gap although the mode overlaps both the poloidal and toroidal gaps. For comparison, the driving term γ was increased slightly to produce no locking as shown by the dashed curve in Fig. 6a. A phase-plane plot of toroidal angle versus velocity is shown in Fig. 6b for the same set of conditions.

We conclude that the MHD mode in MST obeys the sine-Gordon equation. A perturbation analysis predicts locations of mode locking to be at the poloidal and/or toroidal gaps in the vacuum chamber, corresponding to experimental results. Also, mode energy is dissipated when it is locked, as shown by the decaying spiral phase-plane trajectory (Fig. 6b). Finally, locking probability depends on key variables found to be statistically significant using logistical regression. Thus, by varying the key parameters, one can predict the mode locking probability in accord with experiments.

It is a pleasure to thank T. Budimulia and A. K. Hansen for providing the data for the statistical analysis. The authors are especially grateful to S. C. Prager, A. F. Almagri, S. Bisgaard, and R. J. Fonck for their constructive comments and support. This work was supported in part by the U.S. Department of Energy.

[1] R. N. Dexter, D. W. Kerst, T. W. Lovell, S. C. Prager, and J. C. Sprott, Fusion Technol. **19**, 131 (1991).
[2] R. Fitzpatrick, Nucl. Fusion **33**, 1049 (1993).
[3] R. Fitzpatrick and E. P. Yu, Phys. Plasmas **7**, 3610 (2000).
[4] A. Hansen, Ph.D. thesis, University of Wisconsin-Madison, 2000.
[5] C. C. Hegna, Phys. Plasmas **3**, 4646 (1996).
[6] D. W. Hosmer and S. Lemeshow, *Applied Logistic Regression* (John Wiley & Sons, New York, 2000).
[7] T. A. Fulton and R. C. Dynes, Solid State Commun. **12**, 57 (1973).
[8] A. C. Scott, F. Y. F. Chu, and S. A. Reible, J. Appl. Phys. **47**, 3272 (1976).
[9] T. A. Fulton and L. N. Dunkleberger, Appl. Phys. Lett. **22**, 232 (1973).
[10] P. Guéret, IEEE Trans. Magn. **11**, 751 (1975).
[11] D. W. McLaughlin and A. C. Scott, Phys. Rev. A **18**, 1652 (1978).
[12] A. F. Almagri, S. Assadi, S. C. Prager, J. S. Sarff, and D. W. Kerst, Phys. Fluids B **4**, 4080 (1992).